ORIGINAL STUDY

Microstructural study of the Praid Salt Diapir (Transylvanian basin, Romania) and its implication on deformation history and hydrogen storage potential

O. Gelencsér[1,2] · A. Szakács[3] · Á. Gál[4] · Á. Szabó[5] · Z. Dankházi[5] · T. Tóth[6,7] ·
D. Breitner[8] · Zs. Szabó-Krausz[2] · Cs. Szabó[2,9] · Gy. Falus[10]

Abstract

The Transylvanian basin is one of the major Tertiary sedimentary basins in the Carpathian-Pannonian region. Its thick sedimentary fill contains prominent Middle Miocene age salt that forms major diapir structures at the basin margins. The microstructural characteristics of the rock salt represent one of the main factors that determines the potential of a salt body for storage of hydrogen. The main aim of this study is to extend our understanding of the deformation mechanism of Praid rock salt located at the eastern margin of the Transylvanian basin. Based on petrography, we identified two types of rock salt: (1) layered salt with rather uniform grain size distribution showing alternation of greyish (clay mineral bearing) and white (clear halite) layers, and (2) massive grey salt with large, elongated halite crystals, accompanied by sub-micrometer size grains of halite. To shed light on the microstructure of the rock salt, we performed electron backscatter diffraction (EBSD) mapping, and studied gamma-irradiated samples both in the massive and layered salt samples. Dislocation creep and pressure solution creep were identified which acted concurrently in the Praid rock salt. The total strain rate falls between 1.2 and 1.3×10^{-10} s^{-1}. The results of this study reveal a complex deformation history of the salt body where coexisting and migrating fluids have played an important role. The outcome of this project contributes to the hydrogen storage potential assessment for the Transylvanian salt and to a better understanding of the structural evolution of the Transylvanian basin.

Keywords Rock salt · Microstructure · Transylvanian basin · Salt cavern

1 Introduction

1.1 Evaporite texture

Microstructural investigations are currently of great interest in the modern utilization of evaporite rocks (e.g., Ma et al. 2021; Adamuszek et al. 2021). Salt deposits could play a significant role in solving present day challenges such as large-scale hydrogen storage and safe deposition of nuclear waste. The evaluation of these geologic formations needs

---

Extended author information available on the last page of the article

detailed textural observation to help make informed and responsible decisions. Salt is also considered as a model material for inter-metallics, ceramics and rock-forming minerals having high plastic anisotropy (Skrotzki et al. 1995). Experimental determination of the mechanical properties of rock salt and extrapolation of these data to realistic geological conditions have provided a solid basis for understanding the rheology of rock salt (e.g., Urai et al. 1986; Schoenherr et al. 2007).

Microstructural study on Middle Miocene (Badenian) evaporites is almost completely lacking from the scientific literature, although evaporites do play a key role in controlling the dynamical evolution of sedimentary basins (e.g., Urai et al. 1986; Oravecz et al. 2023) such as the Transylvanian basin (TB) in the Carpathian-Pannonian region (CPR). Microstructural studies provide knowledge about the deformation mechanisms affecting the rock salt, hence it contributes to understanding the TB evolution. Thanks to several microstructural studies on rock salt, carried out on synthetic and natural samples worldwide (Guillope and Poirier 1979; Jackson and Talbot 1986; Urai et al. 1986; Zulauf et al. 2010), sufficient literature data are available as a starting point to study the mechanical properties of Badenian salt deposit and make comparison with other deposits of different ages.

In this study the application of gamma-irradiation and electron backscatter diffraction methods were the first and successful attempts to visualize the microstructures of the Transylvanian rock salt. The results are expected to be applicable for quantification of the stress parameters and estimation of the strain rates driving the deformation of the salt body.

1.2 Rock salt as potential storage site

Various types of geological formations can serve as underground storage facilities for resources, and each has its limitation, but their technical and economic viability assessment is still very poor worldwide. Due to its low porosity and permeability, as well as its chemical inertia towards hydrogen, rock salt emerges as a promising candidate for future energy storage sites (Carden and Paterson 1979; Caglayan et al. 2020). The extraction of salt by either classical mining procedures or water leaching to create caverns are regularly used techniques (Allen et al. 1982). Salt caverns are useful for regulating short-term fluctuations in gas consumption and they enable a high rate of gas injection and withdrawal, up to 10–12 cycles a year (Lankof and Tarkowski 2020). However, technical construction of salt caverns depends on several factors: type of salt deposit (undeformed or diapiric), depth of cavern location, mineralogy of the rock salt and technology of mining process (Cyran 2020; Małachowska et al. 2022). The general criteria of underground energy storage for salt domes exploited by water leaching were summarized by Allen et al. (1982): (1) pure rock salt, which is structurally more competent without excess of interbedded insoluble phases (e.g., shales) at a proper depth (200–2000 m) with sufficient thickness (150 m), and; (2) adequate supply of fresh water for leaching the salt, and (3) economically and environmentally acceptable means for brine disposal.

This study is a contribution to better understand the first criterion of Allen et al. (1982), namely, to acquire a detailed structural status and the estimation of the paleo-differential stress of the Praid salt diapir. In fact, the in-situ strength of salt is usually more uniform and consistent than for other types of rocks, but fluid content, mineral impurities, number and distribution of fault zones are some of the geologic factors that affect the expected stability of rock salt. The behavior of the salt is influenced by the depositional environment and loading history, including strain rate, crystal grain boundary state (e.g., wetness), temperature change and loading rate (Matos et al. 2019). In this paper, we studied the deformation

mechanisms operating in Praid rock salt that help in the estimation of cavern convergence (Lankof et al. 2022).

2 Geologic setting

The Transylvanian basin (TB) is located in the Eastern part of the Carpathian-Pannonian region (CPR), surrounded by the Apuseni Mountains and the Eastern and Southern Carpathians (Fig. 1). As one of the most important gas provinces of Eastern Central Europe, it is well explored by boreholes and seismic surveys (e.g., Krézsek et al. 2010).

The main geodynamic processes, determining the landscape of the CPR, are related to the closure of the Neotethys (e.g., Horváth 1993; Schmid et al. 2008). The basement of the TB is formed by the Tisza and Dacia tectonic blocks sutured during the Cretaceous (e.g., Csontos et al. 1992). The TB started to fill up from the Late Cretaceous and its deposition history is strongly related to the evolution of the bordering Carpathian orogen (Krézsek and Filipescu 2005). It is a roughly circular shaped intra-Carpathian basin developed in a back-arc type tectonic setting (e.g., Balintoni et al. 1997; Maţenco et al. 2016). The most significant differences from the much broader Pannonian basin are the followings: the higher thickness of the continental lithosphere (Szafián et al. 1999), the lower heat flux (45 mW/
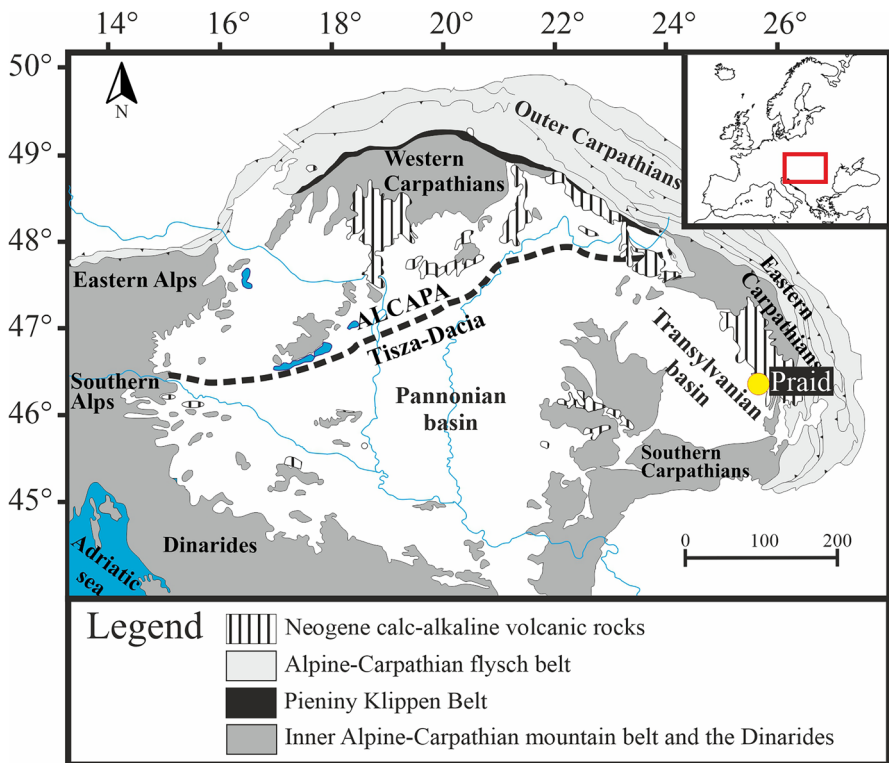
Fig. 1 Simplified geological map of the Carpathian-Pannonian region (CPR) with the assumed ALCAPA–Tisza-Dacia microplate boundary. The yellow dot marks the location of the Praid salt mine. Map is modified after Csontos and Nagymarosy (1998) and references therein

m^2) (Lenkey et al. 2001), and the lack of extensional structures starting from the Miocene (Krézsek and Filipescu 2005; Krézsek and Bally 2006; Tiliţă et al. 2018) in the TB.

The basement of the TB consists of Permian–Jurassic carbonates (dolomites, limestones) and large sheets of supra-subduction ophiolites (Schmid et al. 2008; Tiliţă et al. 2018). Upper Jurassic granitoid intrusions and calc-alkaline volcanics are also intercepted in boreholes (e.g., Ionescu et al. 2009). The Upper Cretaceous sedimentary succession (conglomerates, sandstone, carbonaceous marls and rudist limestone), sealing the basement nappes, has variable thickness (100–1000 m) (Krézsek and Bally 2006). These sedimentary formations are exposed in the Apuseni Mts. and in the South Carpathians (Willingshofer et al. 1999; Schuller 2004).

Initially, in the Paleocene, compressional stress field dominated the area of TB (Fodor et al. 1999), the early basin-filling terrigenous sediments (e.g., Jibou Formation) are sandstones, with evaporitic episodes and shales with a thickness of 500 m (Proust and Hosu 1996). Both shallow marine (~ 100 m) and deeper marine (~ 500–1000 m) deposits were described earlier by Paraschiv (1979).

In the Lower Miocene, the Tisza-Dacia microplate was in the syn-rift phase and moved towards the European Platform. The ALCAPA (Alpine Carpathian Pannonian) microplate thrusted to the Tisza-Dacia resulting in a forearc basin in the northern part of the TB (Csontos and Nagymarosy 1998). Foredeep wedge sediments were recorded in response to the thrusting of ALCAPA. The end of Paleogene was characterized by a large amount of erosion until the offset of the sub-sequent Miocene deposition cycle (Paraschiv 1997; Tiliţă et al. 2018).

The Middle to Late Miocene basin fill is divided into the Badenian, Sarmatian, and Pannonian Stages, reflecting stepwise transitions from normal marine to restricted marine to lacustrine conditions, respectively (Sztanó et al. 2005). The Badenian stage started with marine transgression which was followed by gradual basin deepening (Filipescu and Gîrbacea 1997). Important explosive volcanism-generated volcaniclastic sediments were deposited in submarine environment (Ciulavu et al. 2000; Szakács et al. 2012). The layered, graded complex of volcanoclastic deposits, called Dej Tuff, dated around 15 Ma (Szakács et al. 2012) is overlain by the evaporites subject of this study. The halite–gypsum association is deposited basin-wide with a minor amount of massive, nodular and fibrous gypsum (Ghergari et al. 1991). The average thickness of the evaporite around the basin could be around 300 m (Krézsek et al. 2010). In the Sarmatian, the rock salt was covered by deep marine marls (Krézsek and Bally 2006; Krézsek et al. 2010). Beside marine deposits, sediments with more than one km thickness deposited over the salt layer including products of the subsequent Miocene-Pliocene volcanism (Szakács and Krézsek 2006). The initiation of the volcanism along the eastern margin of the TB could be related to the descent of the Vrancea slab (Sperner et al. 2004; Pécskay et al. 2006). From the Late Miocene to the Quaternary, there were several intensive periods of volcanism resulting in the Eastern Carpathian volcanic chain (Calimani Mts, Gurghiu Mts. and Harghita Mts.) with different petrologic compositions (Szakács and Seghedi 1995; Pécskay et al. 2006; Szakács and Krézsek 2006).

In the TB, many salt diapirs are known e.g., Dej, Turda, Ocna Mureş, Praid, Sovata (Pintea 2008; Har et al. 2010; De Leeuw et al. 2013), the salt outcrops associated with diapirs follow two lineaments NW to SE, and form two diapiric alignments near the eastern and western edges of the TB, respectively (Krézsek and Bally 2006; Bukowski 2013) (Figs. 2, 3). The post-evaporite strata are often affected by salt mobility. Seismic profiles of these structures are illustrated by Krézsek and Bally (2006) and Szakács and Krézsek (2006) as seen in Fig. 3.
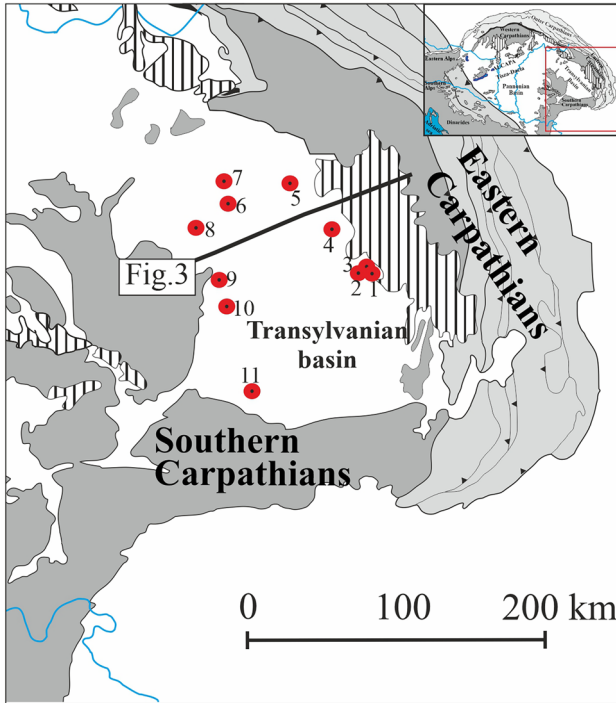
Fig. 2 Cut out of Fig. 1 showing the roughly circular shape Transylvanian basin (TB) and salt outcrops (red dots) at the basin margins. The black line indicates cross section in Fig. 3. Location of salt outcrops: 1 Praid, 2 Sărăţeni, 3 Sovata, 4 Jabeniţa, 5 Sărata, 6 Sic, 7 Ocna Dejului, 8 Cluj-Napoca, 9 Turda, 10 Ocna Mureş, 11 Ocna Sibiului
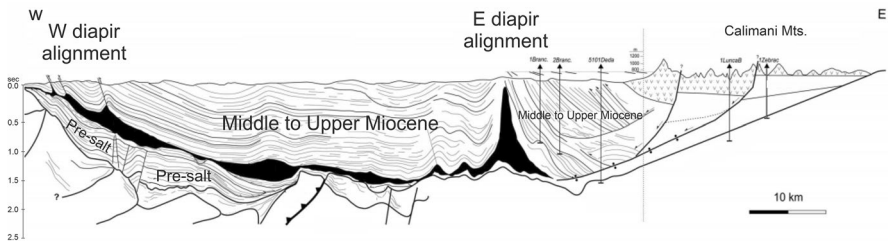
Fig. 3 Seismic interpretation of a W-E section of the Transylvanian basin (TB). For the location, refer to Fig. 2. Black body represents the highly plastic salt layer. The Middle Miocene evaporite forms diapir alignments along the basin margin. Modified after Krézsek and Bally (2006)

In the Pannonian time, the tectonic regime changed to basin inversion, which resulted in general uplift of the TB (e.g., Krézsek and Bally 2006; Tiliţă et al. 2015) and massive deformation and displacement of the rheologically weak sediments (i.e., the salt). The neotectonic inversion is still active presently (e.g., Horváth and Cloetingh 1996; Koroknai et al. 2020). Raw and interpolated stress regimes indicate strike-slip regime in the central part of TB whereas towards the Eastern Carpathians, reverse faulting and transpressional

regimes are dominant (Bada et al. 2007; Békési et al. 2023). The interpolated horizontal stress direction is available for the northern part of the TB indicating E-W trend. The eastern part of CPR (TB, Carpathian foreland, Eastern Carpathians, Southern Carpathians) contributes to the active deformation of the region with a WSW to SSW directed motion (0.5–1.5 mm/yr) contrarywise to the regionally dominant NNE directed motion (2–3 mm/yr) of the Dinarides (Porkoláb et al. 2023). The uplift of the Carpathians led to the formation of Lake Pannon because of the continental collision, which completely cut off the intra-Carpathian realm from the rest of the Paratethys to the end of Late Miocene (Magyar et al. 1999). The lacustrine environment turned to continental setting in the Pleistocene, causing significant erosion (Sztanó et al. 2005) in the whole CPR, at least 500 m sediment could have been eroded (Sanders et al. 2001) in the TB.

3 Materials and methods

3.1 Samples and sample preparation

Hand specimens were collected from the Praid Salt Mine (e.g., boundary pillars and chamber walls). Salt extraction operations excavated a mine in the upper 400 m of the 1.2–1.4 km diameter and 2.7 km high diapir (Horváth 2019) where salt has been exploited for centuries. The observed rock salt can be classified into at least two types, according to their color and structure (Table 1, Fig. 4). One type contains alternating white and grey salt layers, we termed as "layered salt". It shows large scale (tens of meters) folds visible on the chamber walls (Fig. 4b). The other observed salt type shows no visible structure (Fig. 4d, e), except some single vertical cracks filled in with white salt contrasting with the light grey color of the salt mass, terming it as "massive salt" (Table 1). This type has several shades of grey color suggesting the presence of variable amounts of clay minerals besides halite. The contact and lateral extent of the two types of salt was not mapped in detail during this study.

Cutting and polishing of the samples were made in totally dry conditions at the Lithosphere Fluid Research Lab operated at Department of Petrology and Geochemistry, Eötvös Loránd University, Budapest using a Buehler Isomet low-speed saw. The samples were grinded and polished with P800 and P1000 Buehler grinding paper. Thin (50 μm) and thick (> 100 μm) sections were made for petrographic study and textural characterization.

3.2 Polarized microscopy

Petrographic observation was carried out on representative polished thick (~ 1000 μm) and thin sections at the Lithosphere Fluid Research Lab using a Nikon Eclipse E600POL polarized light microscope. Photomicrographs were taken with a Nikon DS Fi1 camera operating with NIS Elements AR 2.20 image editor software.

3.3 Electron backscatter diffraction

Electron backscatter diffraction (EBSD) was used to investigate the microstructure of the studied rock salt. The EBSD method reveals the crystallographic orientation of the individual grains, thus it can help to assess the possible deformation mechanisms which affected the sample. The microstructural study of rock salt requires a sample surface as flat as

Table 1 List of the collected samples from Praid Salt Mine and the applied techniques

Code	Rock salt type	Sampling site	Description	Applied techniques
PA40-2	Layered	Chamber 40	Greyish, translucent, coarse-grained massive rock salt	Stermic, Polmic
PA40-4	Layered	Chamber 40	Clear white, translucent massive halite	Stermic, Polmic, GI
PA40-7	Layered	Chamber 40	Layered rock salt, with alteration of grey and white layers	Stermic, Polmic
PA40-10	Layered	Chamber 40	Layered rock salt, with alteration of grey and white layers (4–5) cm	Stermic, Polmic
PA40-PH	Layered	Chamber 40	Layered rock salt, with alteration of grey (5–8 cm) and white layers (2–5 cm)	Stermic, Polmic, GI, EBSD
PAT17-2	Massive	Telegdy Mine	Greyish, translucent, coarse-grained massive rock salt	Stermic, Polmic, GI
PAT17-3	Massive	Telegdy Mine	Greyish, clayey, coarse-grained massive rock salt	Stermic, Polmic, GI
PAT17-4	Massive	Telegdy Mine	Greyish, translucent, coarse-grained massive rock salt	Stermic, Polmic, EBSD
PAT19-1	Massive	Telegdy Mine	Greyish, translucent, coarse-grained massive rock salt	Stermic, Polmic
PAT19-2	Massive	Telegdy Mine	Greyish, translucent, coarse-grained massive rock salt	Stermic, Polmic
PAT19-3	Massive	Telegdy Mine	Greyish, translucent, coarse-grained massive rock salt	Stermic, Polmic
PAT19-5	Massive	Telegdy Mine	Bright grey massive rock salt with large (> 1 cm) elongated grains	Stermic, Polmic, GI
PAT19-6	Massive	Telegdy Mine	Greyish, translucent, coarse-grained massive rock salt	Stermic, Polmic
PAT19-7	Massive	Telegdy Mine	Greyish, translucent, coarse-grained massive rock salt	Stermic, Polmic, EBSD

Stermic stereo light microscope, *Polmic* polarized light microscope, *EBSD* electron backscatter diffraction, *GI* gamma-irradiation. The detailed location of sampling is provided in the supplementary file
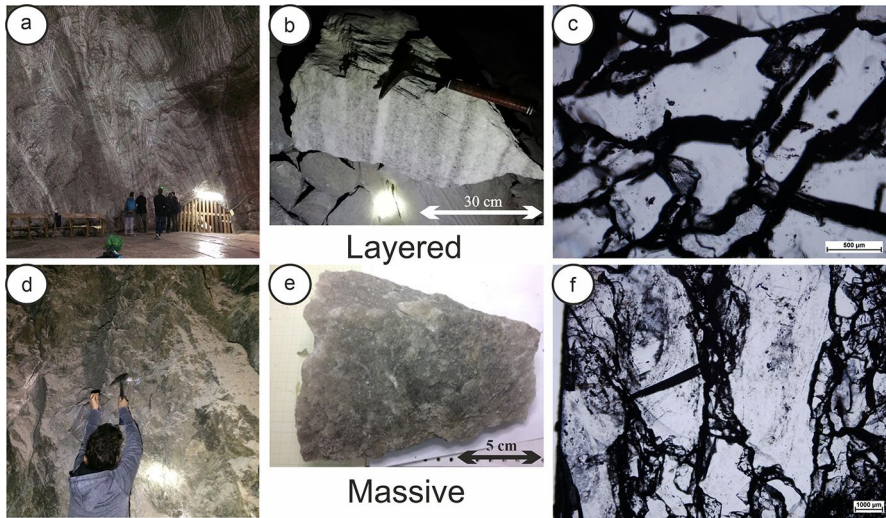
Fig. 4 Characteristic samples from Praid Salt Mine (**a, b**). Layered type rock salt sample and representative thin section (**c**). Grain size distribution is consistent. Approx. 120° junctions are common indicating mosaic structure. **d, e** Massive type rock salt, and photomicrograph (**f**). Elongated large halite crystals (porphyroclasts) are placed in a submillimeter sized crystal mash in massive type salt. Photomicrographs were taken under transmitted light, 1N

possible. Raw samples were cut dry to obtain slabs (ca. $1 \times 1 \times 0.5$ cm) with a precision diamond saw paying high attention to avoid micro-cracking and dissolution artefacts. Then the slab was polished and etched in a slightly undersaturated (~5.5 mol %) NaCl solution for 10 s. Immediately after that, the sample was wiped with a microfiber cloth, then sprayed with n-hexane, and finally dried with pressurized air. These steps were made following Urai et al. (1986) and advice of Jolien Linckens (personal communication 2020).

The EBSD studies were performed on a FEI Quanta 3D scanning electron microscope of the Research and Industrial Relations Center of the Faculty of Science, Eötvös University, Budapest. The electron microscope is equipped with an EDAX Hikari camera and was operated with 4 nA probe current and 20 keV electron beam energy. The sample stage was tilted to 70°. The step size (resolution) of the EBSD map was 15 µm. Data were acquired and evaluated with Orientation Imaging Microscopy (OIM) 7.0 software. The EBSD image quality (IQ) was 43,000 in average and the maximum value was 66,000, showing the majority of the measured points were successfully indexed. The maps were further processed to remove false indexed data (e.g., holes, cracks on the surface) to provide more coherent microstructure maps. The number of removed points were very few (< 1.5%). Further grain and subgrain size evaluation were performed with a python-script (https://github.com/tovask/EBSD/blob/master/filter_and_sum_misorientations.py).

3.4 Gamma-irradiation

Salt samples were cut into slabs ($1 \times 1 \times 0.5$ cm). The microstructure of the salt samples was made visible by gamma-irradiation (GI) experiment which took place at the Radiation Chemistry Department of the Centre for Energy Research, Budapest. The settings of the

irradiation procedure were similar to the ones as described by Urai et al. (1986) and Schléder and Urai (2005). The radiation source was ^{60}Co isotope and the irradiation temperature was ~35 °C. One irradiation was performed at the dose rate of 1–3 kGy/h with a total dose of about 1.5 MGy. The other set was irradiated with a dose rate of 4–6 kGy/h to the total dose of 4 MGy. As a visible result, the salt sample slabs became brown colored heterogeneously. After irradiation, the slabs were polished and etched to remove scratches and provide sub-microscopic relief on the surface. Subgrain structures were examined under the microscope. Quantitative analysis of microstructures was performed to carry out further differential stress and flow law calculations. Grain and subgrain statistics were made with ImageJ software following linear intercept method.

3.5 Differential stress and strain rate estimation

As in other crystalline rocks, polygonal subgrains record the paleostress during steady-state creep because subgrain size is inversely proportional to the peak differential stress (σ):

$$D = k\sigma^{-m}, \tag{1}$$

where D is the average subgrain size in μm. The σ is differential stress in MPa. The k and m are material constants. We used the differential stress calculation of Schléder and Urai (2005) where k and m parameters were derived from experimental data of Carter et al. (1993) and Franssen et al. (1993) based on subgrain piezometry:

$$\sigma = 107D^{-0.87}. \tag{2}$$

Flow laws of salt were constructed based on experiments and theoretical calculations (see Jackson and Hudec 2017 and references therein). Considering steady state, non-dilatant deformation, the flow law of rock salt deformation by steady state dislocation creep is the following:

$$\dot{e}_{DC} = 8.1 \times 10^{-5}\sigma^{4.5}e^{\left(-\frac{51.6}{RT} \times 10^{-3}\right)}, \tag{3}$$

where $\dot{e}_{DC}$ is the strain rate expressed in s^{-1}, 8.1×10^{-5} is a dimensionless pre-exponential material constant, -51.6 (J mol^{-1}) represents the activation energy in the Arrhenius member of the equation, R is the gas constant (J K^{-1} mol^{-1}) and T is temperature in Kelvin (Wawersik and Zeuch 1986; Carter et al. 1993). For rock salt deformation by solution–precipitation creep ($\dot{e}_{PS}$) the following flow law was used:

$$\dot{e}_{PS} = 4.7 \times 10^{-4}e^{\left(-\frac{24.5}{RT} \times 10^{-3}\right)}\left(\frac{\sigma}{Td^3}\right), \tag{4}$$

where 4.7 is a material parameter, -24.5 is activation energy (J mol^{-1}) for pressure-solution creep, σ is the differential stress (MPa), d is the grain diameter (mm) (Spiers et al. 1990; Ter Heege et al. 2005; Urai and Spiers 2007).

4 Results

4.1 Salt and fluid inclusions petrography

The layered type of rock salt is composed of an alternation of grey, clay mineral-rich layers (5–10 cm) and white clay mineral-free halite layers (3–5 cm). The layer boundaries are transitional, the gray and white parts being intercalated. The grain size distribution is fairly consistent (mm in magnitude). Grains are typically subhedral, grain boundaries are usually straightened into polygonal shape (Fig. 4c). Most of the grain boundaries in this type of rock salt contain fluid inclusions. A typical feature is the 120° grain boundary triple junction (Fig. 4c). Primary fabrics such as chevron crystals are missing. This texture tends to have a polygonal mosaic structure as defined by Hardie et al. (1985).

The massive salt type displays deformational fabric, and moderate foliation was observed (Fig. 4f). Large (> 1 cm in size) elongated euhedral grains (porphyroclasts) are surrounded by a sub-millimeter sized halite grain mélange. The porphyroclasts usually contain primary fluid inclusions (FIp) which are representative of the original fluid from which the salt was formed (Roedder 1984a). Relatively small (< 1 mm in size) grains without fluid inclusions compose the mélange (Fig. 4f). The grain size distribution is bimodal, the average grain size ranges between 1.3 and 1.5 mm. Halite grain boundaries are usually euhedral shaped and marked by minerals such as anhydrite, dolomite, and detrital minerals in the clay fraction. The grain boundaries of halite grains sometimes have an irregular lobate morphology. The above-mentioned cm-size elongated grains defined as chevron-like grains usually contain fluid inclusions. The etched surfaces of the samples show polygonal subgrains. Clay minerals are present at the grain boundaries in variable abundance. Where the clay mineral content is higher (> 5 V%), the grain size of halite is relatively smaller than in the clear halite. Some cm-size slightly greenish-colored clay mineral clusters are incorporated in the massive halite matrix (Fig. 4e). This type of rock salt has a slightly protomylonitic texture, similar to Paleogene Iranian rock salt as defined by Schléder and Urai (2007). Both rock salt types are basically monomineralic (halite > 90 V%) but the layered type contains somewhat less clay minerals.

As for the fluid inclusions (FI), in this study the secondary fluid inclusions (FIs) were considered as being representative for post-depositional events. These inclusions are abundant in the samples and occur in various shapes and distributions. Overall, four different FIs types can be distinguished in the studied samples using the definition of Roedder (1984a). The common features shared by FI are the following: they show inter-crystalline distribution, in both massive and layered salt types, cross the grain boundaries, fill the space between crystals. They vary in shape, size and number of phases at room temperature.

- Dark elongated tubular shaped gas-bearing inclusions forming trails are treated as FIs1 type secondary fluid inclusions. They occur in clay mineral-rich halite nearby organic matter. The size of the FIs1 type fluid inclusions varies between 10 and 60 μm (Fig. 5b).
- Fluid inclusions having vermicular-, or amoebae-like shape, containing possibly gas phase are defined as FIs2 type (Fig. 5d). They are characterized by large length/width ratios (1:20–30) and form a network so that it is difficult to distinguish between the connected and the disconnected types of individual inclusions.
- Fluid inclusions with irregular shape and two phases (vapor or vapor + liquid) occurring at cubic cleavage faces of halite are defined as FIs3 type (Fig. 5e). This type of inclu-
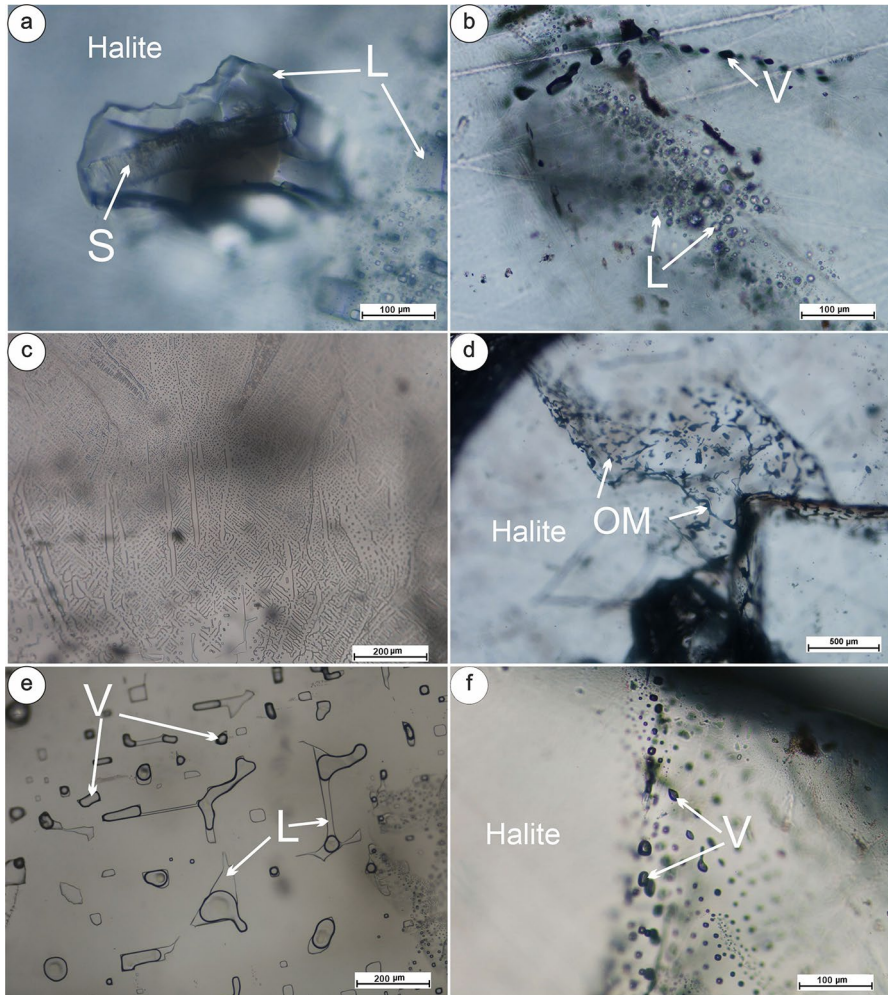
Fig. 5 Photomicrographs of typical secondary fluid inclusions (FI) of the Praid rock salt. FI: fluid inclusion, S: solid, OM: organic matter, L: liquid, V: vapor phases. **a** Fluid inclusion captured tabular anhydrite crystal (S), transmitted light, 1N. **b** Gaseous dark FI array in the vicinity of a primary FIA., transmitted light, 1N. **c** Fluid film at a grain boundary, transmitted light, 1N. **d** Amoebalike FI forming a network, transmitted light, 1N. **e** FI with irregular shape and two phases, transmitted light, 1N. **f** Rounded cubic shaped, gas bearing fluid inclusion trail in halite, transmitted light, 1N

sions displays highly variable shape in their assemblages: from elongated to rounded ones. The size of the inclusions varies from 5 to 100 µm. The phase ratio (vapor/liquid) is variable, necking down and leakage are often observed.

- The fluid inclusions that consistently appear in cubic shape and only contain single vapor phase at room temperature are referred to FIs4 type. This type of inclusions forms trails across grain boundaries and appears along healed fractures. The size of the FIs4 type fluid inclusions varies between 10 and 40 µm. They are very common in both rock salt types (Fig. 5f).

- Beside the well-defined secondary inclusions, mentioned above, there are appearances of fluids at grain boundaries. The shapes of these inter-grain fluid inclusions are often spherical or resemble thin capillaries. The size of them is smaller than 10 μm but they could be even in the submicron size range (Fig. 5c).

Table 2 summarizes the major petrographic and fluid inclusion characteristics of the Praid rock salt.

4.2 Electron backscatter diffraction (EBSD) mapping

EBSD mapping was performed both in massive and layered salt samples to better understand the microstructure of the Praid rock salt. The porphyroclasts contain subgrains with dominant misorientation angle < 2°, a few boundaries between 2° and 5°and, very rarely, with 5°–10°. In the case of layered salt, the subgrain-rich porphyroclasts are surrounded by subgrain-poor equigranular halite crystals. Only a few small (< 1 mm) grains display the lack of substructure. The profiles of both types of rock salt samples (massive and layered), provided on the EBSD maps, show that the degree of misorientation of subgrain boundaries increases from the core of the grain to the edge. Crystallographic preferred orientation (CPO) of the crystals was not observed (Fig. 6).

The average subgrain size slightly differs in the two observed types of salt (Table 3). The massive salt is characterized by 100 μm subgrain size in average, whereas the layered type is characterized by 108 μm subgrain size in average, but with a larger variance. The largest subgrain size (124 μm) was observed in a massive type porphyroclasts-rich sample.

4.3 Images of gamma-irradiated samples

The GI technique was used to study the microstructure of the rock salt as a complementary method to EBSD mapping. Both sets of irradiations, using higher (4 MGy) and lower (1.5 MGy) dose, resulted in the same color change of the samples from darker to brighter brownish.

According to the microstructural observations, samples from the massive salt show fabric made of 1 mm large equigranular subhedral grains with a notable amount of porphyroclasts (5–10 mm). Large numbers of subgrains can be recognized in the porphyroclasts, which are also interlobated by grain boundaries (Fig. 7). The bands are more developed in grains that are adjacent to the large subgrain-rich grains. Porphyroclasts are surrounded by sub-/euhedral grains (~1 mm), which are usually subgrain-poor or seldom subgrain-free.

There are less porphyroclasts in the layered type salt, but subgrain-rich grains and subgrain-poor grains are also present. The grain boundaries, seen as dark lines, are mostly curved and decorated by fluid inclusions (tiny black spots) (Fig. 7).

The obtained subgrain size statistic data are displayed in Table 4. The mean subgrain size of layered and massive salt are about 129 μm and 84 μm, respectively.

Table 2 Summary of the main petrographic and fluid inclusion characteristics of the two rock salt types occurring in the Praid mine

Rock type	Macroscopic features	Microscopic features	Fluid inclusion	Microstructure
Layered	Alternation of grey and white layers	Moderate range in grain size, straight grain contacts at 120° triple junction	Lack of primary fluid inclusions, presence of secondary fluid inclusions	Larger grains having sub-structure smaller grains not having substructure
Massive	Grey colored, cm-size grains, extra-clasts (tuff and clay minerals)	Porphyroclasts are surrounded by submil-limeter sized halite grain mélange, bimodal grain size distribution	Porphyroclasts having primary fluid inclusion in their core, presence of secondary fluid inclusions	Porphyroclasts are subgrain-rich domains, smaller grains not having substructure
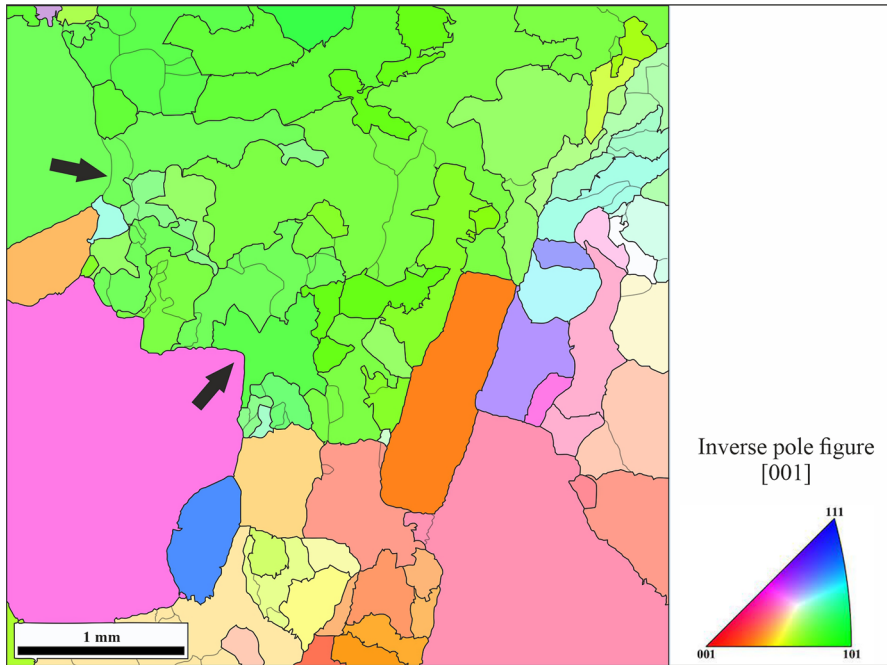
Fig. 6 EBSD map of rock salt shows grains with different crystallographic orientation. Black arrows show the direction of the growing subgrain free grains (green and purple) consume a crystal consisting of subgrains (green). Sample: PAT19-7

Table 3 Quantitative analyses of grain size (in mm) and subgrain size (in μm) performed on rock salt samples (n is the number of analyzed grains, SD is standard deviation)

Sample		Petrography			EBSD mapping		
Type	Code	n	Average grain size (mm)	1 SD	n	Average subgrain size (μm)	1 SD
Layered salt	PA-40	91	1.2	0.8	58	108	58
Massive salt	PAT19-7	108	1.3	1.1	145	100	28

5 Discussion

5.1 Salt deformation

5.1.1 Deformation mechanisms inferred from micropetrography

Rock salt microstructures provide information about the operating deformation mechanism(s) (Guillope and Poirier 1979). Based on petrographic observations, the fabric of the Praid rock salt is dominated by secondary features as it was expected, considering its deformation history (Fig. 2).
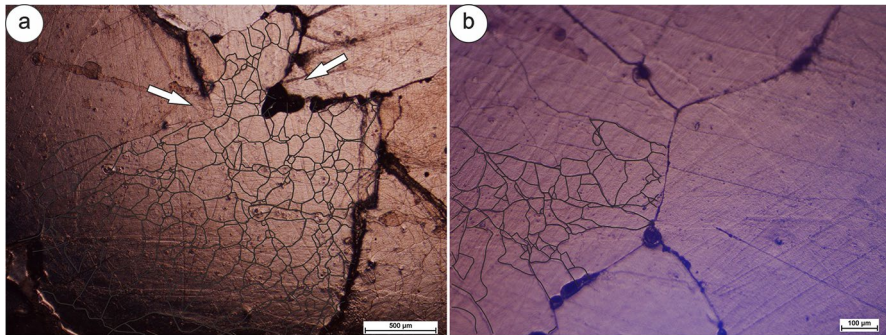
Fig. 7 Surface of the gamma-irradiated rock salt samples. Grain boundaries show up as dark lines, black spots are opened fluid inclusions. **A** Subgrain rich halite grain is consumed by subgrain free grains as indicated by white arrows. Subgrain structure is outlined. Sample: PA40-PH, reflected light. **B** Subgrain rich grain (the left side) in contact with three subgrain free crystals. The network of subgrains is partially outlined. Sample: PAT17-3, reflected light

Table 4 Average subgrain size diameter (in μm) of Praid rock salt based on calculations on gamma-irradiated samples (n is the number of analyzed grains, SD is standard deviation)

Type	Code	n	Average subgrain size (μm)	1 SD
Layered salt	PA-40	46	129	52
Massive salt	PAT17-3	30	84	21

Despite the difference in macroscopic and petrographic scale (namely the presence or the lack of contrasting layers; Table 2, Fig. 4) between the two types of rock salt, they show similarities of their microstructural features (Tables 2, 3, 4). In all the studied samples, subgrain shapes are polygonal, suggesting deformation dominated by climb-controlled creep (Senseny et al. 1992; Schléder and Urai 2005).

The chevron remnants of massive salt samples contain large (1–2 cm in size), subgrain-rich grains. The subgrain-poor (or subgrain-free) grains are characteristically situated adjacent to subgrain-rich halite grains and their elongated shape bulged boundaries, are interpreted as replacing the old grains by grain boundary migration (GBM) (Guillope and Poirier 1979) (Fig. 5). Observations made on both irradiated samples and in EBSD maps also indicate the above-mentioned process (Figs. 6, 7). In many cases, the migrating grain boundaries consume old, milky, fluid inclusion-rich parts of grains (Figs. 6, 7 arrows), which can result in fluid "transport" from the inside of the grains towards grain boundaries (Schléder and Urai 2005).

5.1.2 Differential stress and strain rate estimation

Reliable interpretation of plastic salt deformation during basin evolution requires extrapolation of experimentally derived flow laws to strain rates much lower than those attainable in the laboratory (Urai et al. 2008). One of the common deformation mechanisms in rock salt is the dislocation creep when the crystal distorts by slip along one or more weak crystallographic directions or slip planes, where the lattice is weakly bonded (Jackson

Table 5 Selected rock salt deposits of different geological settings with examined halite grain sizes (mm) and differential stress (MPa)

References	Mean average grain size (mm)	Mean differential stress (MPa)	Locality	Geological setting
This study (layered salt)	1.2	1.8	Praid (Transylvania, Romania)	Salt diapir
This study (massive salt)	1.4	2.0		
Thiemeyer et al. (2016)	3.4	1.1–1.3	Gorleben (Germany)	Salt diapir
Kneuker et al. (2014)	<5	1.2–2.9	Morsleben (Germany)	Salt diapir
Mertineit et al. (2014)	0.3–2.5	2.28–2.97	Gorleben (Germany)	Salt diapir
Schléder et al. (2007)	3–25	0.9–3.1	Kłodawa (Poland)	Salt diapir
Schoenherr (2008)	2–30	<2	Birba, Harweel (Oman)	Salt diapir
Tămaş et al. (2021)	1.5	4	Mânzăleşti (Romania)	Salt diapir
Desbois et al. (2010)	<0.5	3.1–4.8	Qum Kuh (Iran)	Salt fountain

Table 6 Calculated differential stress (MPa) and strain rates (s^{-1}) obtained from Eqs. (3) and (4). The higher strain rate belongs to the solution precipitation creep in both rock types

Rock type	Differential stress (MPa)	Flow laws	
		Dislocation creep (s^{-1})	Solution-precipitation creep (s^{-1})
Layered salt	1.8	5.1×10^{-12}	1.3×10^{-10}
Massive salt	2.0	8.8×10^{-12}	1.2×10^{-10}

and Hudec 2017). Under conditions of long-term deformation, grain boundary dissolution–precipitation processes, such as solution-precipitation creep (or "pressure solution") and dynamic recrystallisation, play a significant role (Urai et al. 2008). The calculated differential stress values from Praid are in the range of typical domal salt data (Table 5 and references within).

Based on the detailed microstructural observations, we suggest that both dislocation creep and pressure solution processes act concurrently in the Praid rock salt. This flow law is a precise formulation, but for a given differential stress, the rate of dislocation creep can vary by about three orders of magnitude because of differences in solid solution impurities, secondary minerals, grain size, dislocation density and fluids in grain boundaries (Urai and Spiers 2007; Jackson and Hudec 2017).

The pressure solution creep is strongly dependent on grain size, whereas dislocation creep deformation is grain size independent. Since there is no available data about paleo geothermal temperature values, the present-day value was used (~30 °C/km), (Demetrescu et al. 2001; Asimopolos and Asimopolos 2018), T = 315 K in the calculations.

The total strain rate is given by the sum of dislocation creep (DC) and pressure solution (PS) strain rates:

$$\dot{e} = \dot{e}_{DC} + \dot{e}_{PS} \tag{5}$$

In the Praid samples, the strain rate of DC creep plays a minor role compared to the SP creep (Table 6).

5.2 Interpretation of secondary features

Based on the petrographic observations and microstructural study presented above, a concept is drawn up for the microscale processes by which the Badenian salt of the TB deformed. The initial burial of the salt may induce only slight deformations in the primary fabric as it was concluded in Lowenstein and Hardie (1985) when they compared modern and ancient shallow buried halites. The macroscopic dissimilarities, presence or lack of layers, might be originated from the different depositional environment. Original chevron-type grains, (referred to as porphyroclasts in this study), containing primary fluid inclusions were probably more abundant, with a notable amount of fluids at the early stage of salt deformation (Fig. 4f). Unfortunately, the contact of the rock salt types (massive and layered halite) has not been observed in the Praid mine, however, it would have been essential in the interpretation of their original relationship in both space and time.

Subsequently, the organic materials started to decompose and possibly converted into carbohydrates, which were trapped in fluid inclusions (Fig. 5b, d) as happened in the cases of the Ara salt in Oman (Schoenherr et al. 2007) and the Port-Gentil salt diapir in Gabon (Pironon et al. 1995).

Due to the increasing differential stress and temperature, the syn-depositional fluid inclusion-rich halite crystals were partially or totally recrystallized, and their fluids were added to the pore fluid by the grain boundary migration process (Drury and Urai 1990). During this process, the grain boundary fluids (including those originating from decomposed organic material) started to form continuous fluid films bordering the grains (Fig. 5c) and wormlike tubes (Fig. 5d), respectively. This stage of deformation may be related to the growth of the Praid diapir and Neogene tectonic activity of the study area when the main driving mechanisms could be the compressional forces (Ranete and Maţenco 2013). The volcanic activity nearby could also enhance the rock salt deformation and diapirism by both its loading and thermal effect (Szakács and Krézsek 2006).

It is expected that while a grain boundary sweeps through a milky and fluid inclusion-rich crystal it collects the available fluid inclusions. This process could continue until the driving force ceased. As our results show, pressure solution creep played a significant role in halite alongside dislocation creep process.

Because the recent depth of the sampled rocks is shallow (< 200 m from the surface), it is possible that the salt layer was affected by a higher than recent temperature gradient caused by nearby Late Miocene volcanism (Krézsek and Bally 2006; Szakács and Krézsek 2006) and along with temperature increase related to burial depth (of 800–1000 m). As the salt body moved upwards to near-surface position, in parallel differential stress was likely to decrease, and the creep processes became less pronounced. Fluid films still exist in the samples, thus the diffusional processes are still assumed to be active (Fig. 5c).

Furthermore, the paleo-differential stress calculations on the Praid rock salt samples indicate a maximum differential stress less than 1.8 MPa for layered salt and less than 2 MPa for massive salt. These values are in accordance with the dataset of diapiric salt-related stress values worldwide (Carter et al. 1993; Schoenherr et al. 2007; Table 5). Based on our petrographic observation and EBSD mapping, we assume that the dominant deformation mechanism is the solution precipitation creep. The strain rate calculations (total strain rate between 1.2 and 1.3×10^{-10} s^{-1}) suggest relatively fast movements in the diapir body.

5.3 Praid as a potential storage site

The scientific papers estimating rock salt potential around Europe usually do not consider the Transylvanian salt as a potential storage site for hydrogen. Iordache et al. (2014) made a preliminary study in Romania mentioning no Transylvanian salt occurrences among the candidates. In a more recent study, the Tertiary (including Badenian) salt deposits are missing from the list of potential storage sites due to their highly deformed structure (Caglayan et al. 2020). However, parameters of the hydrogen storage in salt caverns will ultimately depend on the needs of investors and will require detailed analyzes at the cavern design stage (Lankof et al. 2022).

Considering the criteria of radioactive waste disposal, long-term stable geological conditions are essential. Safe nuclear waste disposal in salt requires a fundamental understanding of its mechanical behavior to predict performance of nuclear waste repositories for longer time (million years) than those usually encountered in conventional geotechnical practice (Roedder 1984b; Senseny et al. 1992). For seasonal energy storage, the horizontal stress should not exceed 120 % of overburden pressure. Assuming 100% dense rock above the rock salt at depth of 800 m, the overburden pressure would be 16.9 MPa (Allen et al. 1982; Matos et al. 2019). Furthermore, a cavern boundary creep strain of 10% is considered as acceptable limit of safety for compressed air energy storage. The observed strain of Praid rock salt might be acceptable as relevant for the ongoing deformation of the salt body, but additional microstructural results are needed to be obtained for a more robust assessment of the salt diapir. Moreover, there are other criteria for gas storage capability (including e.g., economical, ecological) whose discussion is beyond the scope of this paper.

Taking into account the current status of the Praid salt diapir (i.e., a protected area hosting active mining and tourism and leisure activities) underground hydrogen storage is not considered as a realistic project in the near future. However, the results obtained in our study may help planning, devising, and realizing hydrogen storage spaces in other voluminous salt diapir bodies of the same evaporite-hosting province in Transylvania, having identical origin, deformation history and rock salt characteristics, as well as a similar mining history and technology including currently inactive underground cavities left behind after salt extraction ceased.

6 Conclusions

A detailed microstructural study was carried out on Middle Miocene rock salt of the Praid diapir from the eastern Transylvanian basin in Romania. The salt mass is tectonically reworked, and two types of rock salt were distinguished in the salt dome. Layered salt has alternating clay mineral-rich and -poor layers. The grains usually have 120° grain boundary triple junctions. The texture of the massive salt is characterized as protomylonitic texture where large porphyroclastic halites are surrounded by sub-millimeter size halite grains.

Petrographic (rock and fluid inclusion) results reveal a complex deformation history of the salt body as evidenced by subgrain formation and recrystallization in the rock salt where coexisting and migrating fluids have played important role. Microfabric data, obtained from gamma-irradiated samples and EBSD measurements, are in line with the

assumption that halite deformation was accommodated by deformation mechanisms, both dislocation creep and solution-precipitation creep.

The identification of the various microstructures helps to understand the operating deformation mechanisms in rock salt, which were active during salt diapir emplacement at Praid. Hence microstructural studies could be helpful in future developing strategies of hydrogen storage sites and mine maintenance by providing insights into the stability of the Praid rock salt.

Author contributions Conceptualization: [OG, GF]; Methodology: [OG, GF, CS]; Formal analysis and investigation: [OG, ÁS, GF]; Visualization: [OG]; Writing—original draft preparation: [OG]; Writing—review and editing: [GF, CS, AS, ÁG, ZS-K, ZD, TT]; Funding acquisition: [GF, DB]; Resources: [CS, ZD, TT]; Supervision: [GF, CS].

Declarations

Conflict of interest The authors have no conflict of interest to declare that are relevant to the content of this article.

References

Adamuszek M, Tămaş DM, Barabasch J, Urai JL (2021) Rheological stratification in impure rock salt during long-term creep: morphology, microstructure, and numerical models of multilayer folds in the Ocnele Mari salt mine, Romania. Solid Earth 12(9):2041–2065

Allen RD, Doherty TJ, Thoms RL (1982) Factors affecting storage of compressed air in solution mined salt cavities. Proc Intersoc Energy Convers Eng Conf 4:1992–1999

Asimopolos N-S, Asimopolos L (2018) Study on the geothermal energy on Romanian territory. Prog Cryog Isot Sep 21:43–48

Bada G, Horváth F, Dövényi P, Szafián P, Windhoffer G, Cloetingh S (2007) Present-day stress field and tectonic inversion in the Pannonian basin. Glob Planet Change 58(1–4):165–180. https://doi.org/10.1016/j.gloplacha.2007.01.007

Balintoni I, Seghedi I, Szakács A (1997) Review of the Neogene post-collisional magmatism tectonics interplay in the intracarpathian region. Stud Univ Babeş-Bolyai Ser Geol Cluj-Napoca 42:33–49

Békési E, Porkoláb K, Wesztergom V, Wéber Z (2023) Updated stress dataset of the Circum-Pannonian region: implications for regional tectonics and geo-energy applications. Tectonophysics 856:229860

Bukowski K (2013) Chapter 2. Salt sources and salt springs in the Carpathian zone. In: Archaeolingua, p 9

Caglayan DG, Weber N, Heinrichs HU, Linßen J, Robinius M, Kukla PA, Stolten D (2020) Technical potential of salt caverns for hydrogen storage in Europe. Int J Hydrog Energy 45:6793–6805. https://doi.org/10.1016/j.ijhydene.2019.12.161

Carden PO, Paterson L (1979) Physical, chemical and energy aspects of underground hydrogen storage. Int J Hydrog Energy 4:559–569

Carter NL, Horseman ST, Russell JE, Handin J (1993) Rheology of rocksalt. J Struct Geol 15:1257–1271

Ciulavu D, Dinu C, Szakacs A, Dordea D (2000) Neogene kinematics of the Transylvanian basin (Romania). Am Assoc Pet Geol Bull 84:1589–1615

Csontos L, Nagymarosy A (1998) The Mid-Hungarian line: a zone of repeated tectonic inversions. Tectonophysics 297:51–71

Csontos L, Nagymarosy A, Horvath F, Kovac M, Tari G (1992) Tertiary Kinematics of the Intra-Carpathian Area

Cyran K (2020) Insight into a shape of salt storage caverns. Arch Min Sci 65:363–398

Demetrescu C, Nielsen SB, Ene M, Şerban DZ, Polonic G, Andreescu M, Pop A, Balling N (2001) Lithosphere thermal structure and evolution of the Transylvanian depression: insights from new geothermal measurements and modelling results. Phys Earth Planet Int 126:249–267

Desbois G, Závada P, Schléder Z, Urai JL (2010) Deformation and recrystallization mechanisms in actively extruding salt fountain: microstructural evidence for a switch in deformation mechanisms with increased availability of meteoric water and decreased grain size (Qum Kuh, central Iran). J Struct Geol 32:580–594

Drury RM, Urai JL (1990) Deformation-related recrystallization processes. Tectonophysics 172:235–253

Filipescu S, Gîrbacea R (1997) Lower Badenian sea-level drop on the western border of the Transylvanian Basin: foraminiferal paleobathymetry and stratigraphy. Geol Carpathica 48:325–334

Fodor L, Csontos L, Bada G, Györfi I, Benkovics L (1999) Tertiary tectonic evolution of the Pannonian Basin system and neighbouring orogens: a new synthesis of palaeostress data. Geol Soc Spec Publ 156:295–334

Franssen RCMW (1993) Rheology of synthetic rocksalt with emphasis on the influence of deformation history and geometry on the flow behaviour. PhD thesis, Rijksuniversiteit Utrecht

Ghergari L, Mészáros N, Hosu A, Filipescu S, Chira C (1991) The gypsiferous formation at Cheia (Cluj County). Stud Univ Babes-Bolyai Ser Geol 36:13–28

Guillope M, Poirier JP (1979) Dynamic recrystallization during creep of single-crystalline halite: an experimental study. J Geophys Res 84:5557–5567

Har N, Rusz O, Codrea V, Barbu O (2010) New data on the mineralogy of the salt deposit from Sovata (Mures county-Romania). Carpathian J Earth Environ Sci 5:127–135

Hardie LA, Lowenstein TK, Spencer RJ (1985) The problem of distinguishing between primary and secondary features in evaporites. Sixth Int Symp Salt 1:173–195

Ter Heege JH, De Bresser JHP, Spiers CJ (2005) Dynamic recrystallization of wet synthetic polycrystalline halite: Dependence of grain size distribution on flow stress, temperature and strain. Tectonophysics 396:35–57

Horváth F (1993) Towards a mechanical model for the formation of the Pannonian basin. Tectonophysics 226:333–357

Horváth F, Cloetingh S (1996) Stress-induced late-stage subsidence anomalies in the Pannonian basin. Tectonophysics 266(1–4):287–300. https://doi.org/10.1016/S0040-1951(96)00194-1

Horváth I (2019) A parajdi sóbánya titkai, 1. http://www.salinapraid.ro/tortenelem-kitermeles. Accessed 5 May 2020.

Iordache I, Schitea D, Gheorghe AV, Iordache M (2014) Hydrogen underground storage in Romania, potential directions of development, stakeholders and general aspects. Int J Hydrog Energy 39:11071–11081. https://doi.org/10.1016/j.ijhydene.2014.05.067

Jackson MPA, Hudec MR (2017) Salt tectonics: Principles and practice. Cambridge University Press, Cambridge

Jackson MPA, Talbot CJ (1986) External shapes, strain rates, and dynamics of salt structures. Geol Soc Am Bull 97:305–323

Kneuker T, Zulauf G, Mertineit M, Behlau J, Hammer J (2014) Deformationsverhalten von permischen Staßfurt-Steinsalz aus Morsleben (Deutschland) bei unterschiedlichem finitem strain: Abschätzungen aus mikrogefüge-studien und EBSD-analysen. Zeitschrift Der Dtsch Gesellschaft Für Geowissenschaften 165:91–106

Koroknai B, Wórum G, Tóth T, Koroknai Zs, Fekete-Németh V, Kovács G (2020) Geological deformations in the Pannonian Basin during the neotectonic phase: new insights from the latest regional mapping in Hungary. Earth Sci Rev 211:103411. https://doi.org/10.1016/j.earscirev.2020.103411

Krézsek C, Bally AW (2006) The Transylvanian Basin (Romania) and its relation to the Carpathian fold and thrust belt: Insights in gravitational salt tectonics. Mar Pet Geol 23:405–442

Krézsek C, Filipescu S (2005) Middle to late Miocene sequence stratigraphy of the Transylvanian Basin (Romania). Tectonophysics 410:437–463

Krézsek C, Filipescu S, Silye L, Maţenco L, Doust H (2010) Miocene facies associations and sedimentary evolution of the Southern Transylvanian Basin (Romania): implications for hydrocarbon exploration. Mar Pet Geol 27:191–214

Lankof L, Tarkowski R (2020) Assessment of the potential for underground hydrogen storage in bedded salt formation. Int J Hydrog Energy 45:19479–19492. https://doi.org/10.1016/j.ijhydene.2020.05.024

Lankof L, Urbańczyk K, Tarkowski R (2022) Assessment of the potential for underground hydrogen storage in salt domes. Renew Sustain Energy Rev 160:112309

De Leeuw A, Filipescu S, Maţenco L, Krijgsman W, Kuiper K, Stoica M (2013) Paleomagnetic and chronostratigraphic constraints on the middle to late miocene evolution of the transylvanian basin (Romania): implications for central paratethys stratigraphy and emplacement of the tisza-dacia plate. Glob Planet Change 103:82–98

Lenkey L, Dövényi P, Horváth F, Cloetingh SAPL (2001) Geothermics of the Pannonian basin and its bearing on the neotectonics. Stephan Mueller Spec Publ Ser 3:29–40

Lowenstein TK, Hardie LA (1985) Criteria for the recognition of salt-pan evaporites. Sedimentology 32(5):627–644

Ma X, Xu Z, Chen L, Shi X (2021) Creep deformation analysis of gas storage in salt caverns. Int J Rock Mech Min Sci 139:104635

Magyar I, Geary DH, Sütő-Szentai M, Lantos M, Müller P (1999) Integrated biostratigraphic, magnetostratigraphic and chronostratigraphic correlations of the Late Miocene Lake Pannon deposits. Acta Geol Hungarica 42:5–31

Małachowska A, Łukasik N, Mioduska J, Gębicki J (2022) Hydrogen storage in geological formations—the potential of salt caverns. Energies 15:1–19

Maţenco L, Munteanu I, ter Borgh M, Stanica A, Tiliţă M, Lericolais G, Dinu C, Oaie G (2016) The interplay between tectonics, sediment dynamics and gateways evolution in the Danube system from the Pannonian Basin to the western Black Sea. Sci Total Environ 543:807–827. https://doi.org/10.1016/j.scitotenv.2015.10.081

Matos CR, Carneiro JF, Silva PP (2019) Overview of large-scale underground energy storage technologies for integration of renewable energies and criteria for reservoir identification. J. Energy Storage 21:241–258. https://doi.org/10.1016/j.est.2018.11.023

Mertineit M, Schramm M, Hammer J, Zulauf G (2014) Deformation of anhydrite rocks (Gorleben-Bank, z3OSM) in a high-strain domain of the Gorleben salt dome, Germany. Zeitschrift Der Dtsch Gesellschaft Für Geowissenschaften 165:49–62

Oravecz É, Héja G, Fodor L (2023) Salt tectonics versus shortening: recognizing pre-orogenic evaporite deformation in salt-bearing fold-and-thrust belts on the example of the Silica Nappe (Inner Western Carpathians). Tectonics 42(8):e2023TC007842

Paraschiv D (1979) Romanian oil and gas fields. Institute of Geology and Geophysics, Bucharest

Paraschiv D (1997) The pre-Paratethys buried denudational surface in Romanian territory. Rev Roum Géographie 41:21–32

Pécskay Z, Lexa J, Szakács A, Seghedi I, Balogh K, Konečný V, Zelenka T, Kovacs M, Póka T, Fülöp A, Márton E, Panaiotu C, Cvetković V (2006) Geochronology of Neogene magmatism in the Carpathian arc and intra-Carpathian area. Geol Carpathica 57:511–530

Pintea I (2008) Liquid inclusions microthermometry in the Badenian halite and actual evaporite salt crust from Romania. Rom J Miner Depos 83:115–118

Pironon J, Pagel M, Walgenwitz F, Barrès O (1995) Organic inclusions in salt. Part 2: oil, gas and ammonium in inclusions from the Gabon margin. Org Geochem 23:739–750

Porkoláb K, Broerse T, Kenyeres A, Békési E, Tóth S, Magyar B, Wesztergom V (2023) Active tectonics of the Circum-Pannonian region in the light of updated GNSS network data. Acta Geod Geophys 58:1–25. https://doi.org/10.1007/s40328-023-00409-8

Proust JN, Hosu A (1996) Sequence stratigraphy and Paleogene tectonic evolution of the Transylvanian Basin (Romania, eastern Europe). Sediment Geol 105:117–140

Ranete E, Maţenco L (2013) Salt tectonics on the eastern side of the Transylvanian Basin, Romania. EAGE 13:2–4

Roedder E (1984a) Fluid inclusions: an introduction to studies of all types of fluid inclusions, gas, liquid, or melt, trapped in materials from earth and space, and their application to the understanding of geologic processes. Mineralogical Society of America, Chantilly

Roedder E (1984b) The fluids in salt. Am Mineral 69:413–439

Sanders C, Huismans R, van Wees JD, Andriessen P (2001) The Neogene history of the Transylvanian basin in relation to its surrounding mountains. Stephan Mueller Spec Publ Ser 3:121–133

Schléder Z, Burliga S, Urai JL (2007) Dynamic and static recrystallization-related microstructures in halite samples from the Kłodawa salt wall (central Poland) as revealed by gamma-irradiation. Neues Jahrb Fur Mineral Abhandlungen 184:17–28

Schléder Z, Urai JL (2007) Deformation and recrystallization mechanisms in mylonitic shear zones in naturally deformed extrusive Eocene-Oligocene rocksalt from Eyvanekey plateau and Garmsar hills (central Iran). J Struct Geol 29:241–255

Schléder Z, Urai JL (2005) Microstructural evolution of deformation-modified primary halite from the Middle Triassic Röt Formation at Hengelo, The Netherlands. Int J Earth Sci 94:941–955

Schmid SM, Bernoulli D, Fügenschuh B, Maţenco L, Schefer S, Schuster R, Tischler M, Ustaszewski K (2008) The Alpine-Carpathian-Dinaridic orogenic system: correlation and evolution of tectonic units. Swiss J Geosci 101:139–183

Schoenherr J (2008) The Evolution of Halite and Solid Bitumen in the Petroleum System of the South Oman Salt Basin. Geol Endog Dynamik PhD. Available at: http://darwin.bth.rwth-aachen.de/opus3/frontdoor.php?source_opus=2131&la=de.

Schoenherr J, Urai JL, Kukla PA, Littke R, Schléder Z, Larroque JM, Newall MJ, Al-Abry N, Al-Siyabi HA, Rawahi Z (2007) Limits to the sealing capacity of rock salt: a case study of the infra-Cambrian Ara Salt from the South Oman salt basin. Am Assoc Pet Geol Bull 91:1541–1557

Schuller V (2004) Evolution and geodynamic significance of the Upper Cretaceous Gosau basin in the Apuseni Mountains (Romania). University of Tübingen

Senseny PE, Hansen FD, Russell JE, Carter NL, Handin JW (1992) Mechanical behaviour of rock salt: phenomenology and micromechanisms. In International journal of rock mechanics and mining sciences and geomechanics abstracts. Elsevier, pp 363–378

Skrotzki W, Helming K, Brokmeier H-G, Dornbusch H-J, Welch P (1995) Textures in pure shear deformed rock salt. Textures Microstruct 24:133–141

Sperner B, Ioane D, Lillie RJ (2004) Slab behaviour and its surface expression: new insights from gravity modelling in the SE-Carpathians. Tectonophysics 382:51–84

Spiers CJ, Schutjens PMTM, Brzesowsky RH, Peach CJ, Liezenberg JL, Zwart HJ (1990) Experimental determination of constitutive parameters governing creep of rocksalt by pressure solution. Geol Soc Spec Publ 54:215–227

Szafián P, Tari G, Horváth F, Cloetingh S (1999) Crustal structure of the Alpine-Pannonian transition zone: a combined seismic and gravity study. Int J Earth Sci 88:98–110

Szakács A, Krézsek C (2006) Volcano-basement interaction in the Eastern Carpathians: Explaining unusual tectonic features in the Eastern Transylvanian Basin, Romania. J Volcanol Geotherm Res 158:6–20

Szakács A, Pécskay Z, Silye L, Balogh K, Vlad D, Fülöp A (2012) On the age of the Dej Tuff, Transylvanian Basin (Romania). Geol Carpathica 63:139–148

Szakács A, Seghedi I (1995) The Calimani-Gurghiu-Harghita volcanic chain, East Carpathians, Romania: volcanological features. Acta Vulcanol 7:145–153

Sztanó O, Krézsek C, Magyar I, Wanek F, Juhász G (2005) Sedimentary cycles and rhythms in a Sarmatian to Pannonian (Late Miocene) transitional section at Oarba de Mures/Marosorbó. Transylvanian Basin Acta Geol Hungarica 48:235–257

Tămaş DM, Tămaş A, Barabasch J, Rowan MG, Schléder Z, Krézsek C, Urai JL (2021) Low-angle shear within the exposed Mânzăleşti Diapir, Romania: salt decapitation in the Eastern Carpathians Fold-and-Thrust Belt. Tectonics 40:e2021TC006850

Thiemeyer N, Zulauf G, Mertineit M, Linckens J, Pusch M, Hammer J (2016) Microfabrics and 3D grain shape of Gorleben rock salt: constraints on deformation mechanisms and paleodifferential stress. Tectonophysics 676:1–19. https://doi.org/10.1016/j.tecto.2016.02.046

Tiliţă M, Lenkey L, Maţenco L, Horváth F, Surányi G, Cloetingh S (2018) Heat flow modelling in the Transylvanian basin: Implications for the evolution of the intra-Carpathians area. Glob Planet Change 171:148–166

Tiliţă M, Scheck-Wenderoth M, Maţenco L, Cloetingh S (2015) Modelling the coupling between salt kinematics and subsidence evolution: inferences for the Miocene evolution of the Transylvanian Basin. Tectonophysics 658:169–185. https://doi.org/10.1016/j.tecto.2015.07.021

Urai JL, Spiers CJ (2007) Deformation mechanisms and rheology of halite in experiments. SaltMech 6:22–25

Urai JL, Spiers CJ, Zwart HJ, Lister GS (1986) Weakening of rock salt by water during long-term creep. Nature 324:554–557

Urai JL, Schléder Z, Spiers CJ, Kukla PA (2008) Flow and transport properties of salt rocks. Dynamics of complex intracontinental basins: the central European basin system. Springer Berlin, Heidelberg

Wawersik WR, Zeuch DH (1986) Modeling and mechanistic interpretation of creep of rock salt below 200 °C. Tectonophysics 121:125–152

Willingshofer E, Neubauer F, Cloetingh S (1999) The significance of Gosau-type basins for the Late Cretaceous tectonic history of the Alpine-Carpathian belt. Phys Chem Earth Part A Solid Earth Geod 24:687–695

Zulauf G, Zulauf J, Bornemann O, Brenker FE, Höfer HE, Peinl M, Woodland AB (2010) Experimental deformation of a single-layer anhydrite in halite matrix under bulk constriction. Part 2: deformation mechanisms and the role of fluids. J Struct Geol 32:264–277

Authors and Affiliations

O. Gelencsér[1,2] ⦿ **· A. Szakács[3] · Á. Gál[4] · Á. Szabó[5] · Z. Dankházi[5] · T. Tóth[6,7] · D. Breitner[8] · Zs. Szabó-Krausz[2] · Cs. Szabó[2,9] · Gy. Falus[10]**

✉ O. Gelencsér
gecso@staff.elte.hu

1   Doctoral School of Environmental Sciences, ELTE Eötvös Loránd University, Budapest, Hungary

2   Lithosphere Fluid Research Lab, ELTE Eötvös Loránd University, Budapest, Hungary

3   Institute of Geodynamics, Romanian Academy, Bucharest, Romania

4   Babeş-Bolyai University, Cluj-Napoca, Romania

5   Department of Material Physics, ELTE Eötvös Loránd University, Budapest, Hungary

6   HUN-REN Centre for Energy Research, Budapest, Hungary

7   Department of Organic Chemistry and Technology, Faculty of Chemical Technology and Biotechnology, Budapest University of Technology and Economics, Budapest, Hungary

8   Green Ventures Ltd., Budapest, Hungary

9   HUN-REN Institute of Earth Physics and Space Science, Sopron, Hungary

10 Supervisory Authority for Regulatory Affairs, Budapest, Hungary